Desalination and Water Treatment
www.deswater.com

doi: 10.5004/dwt.2017.0529

62 (2017) 273–281
February

Development of activated carbon from *Phoenix dactylifera* fruit pits: process optimization, characterization, and methylene blue adsorption

Abdullah Aldawsari[a], Moonis Ali Khan[a,*], B.H. Hameed[b], Zeid Abdullah AlOthman[a], Masoom Raza Siddiqui[a], A. Yacine Badjah Hadj Ahmed[a], Ibrahim Hotan Alsohaimi[a]

[a]*Department of Chemistry, College of Science, King Saud University, P.O. Box 2455, Riyadh 11451, Saudi Arabia, emails: moonisalikhan@gmail.com, mokhan@ksu.edu.sa (M.A. Khan), alfraj2008@hotmail.com (A. Aldawsari), zaothman@ksu.edu.sa (Z. AlOthman), siddiqui124@gmail.com (M.R. Siddiqui), ybadjah@ksu.edu.sa (A.Y.B.H. Ahmed), chem-ihg@hotmail.com (I.B. Alsohaimi)*
[b]*School of Chemical Engineering, Engineering Campus, Universiti Sains Malaysia, 14300 Nibong Tebal, Penang, Malaysia, email: chbassim@usm.my (B.H. Hameed)*

Received 5 July 2016; Accepted 18 July 2016

ABSTRACT

Herein, Date Pit Char (DPC) was chemically activated by Alkaline Metal Hydroxides (AMHs) viz. NaOH and KOH. Impregnation ratio and activation temperature were optimized. Among AMHs, NaOH was selected for DPC activation achieving highest yield (56.77%) and maximum methylene blue (MB) adsorption (100 mg/g) for sample DPAC11 with impregnation ratio–3:1 and activation temperature–800°C. Textural properties, surface morphology, elemental content, and surface functional groups were explored to characterize DPAC11. The observed BET surface, total pore volume, and average pore size of DPAC11 were 377.63 m^2/g, 0.0275 cm^3/g, and 21.17 Å, respectively. Presence of both micro- and meso-pores on DPAC11 surface was depicted by N_2 adsorption/desorption isotherm. Batch mode MB adsorption studies were carried out. Results showed thermodynamically favorable adsorption, fitted to Langmuir isotherm and pseudo-second-order kinetic models with maximum monolayer adsorption capacities varied between 104.02 and 146.29 mg/g for temperature range 303–323 K, respectively. No significant effect of pH on adsorption was observed. The observed equilibration time for MB C_0 range 25–200 mg/L was in between 240 and 600 min, accomplishing 23% to 60% MB adsorption within initial 30 min. Hence, it could be concluded that DPAC11 is a potential adsorbent for rapid and effective removal of MB from aqueous phase.

Keywords: Activated carbon; Date pits; Adsorption; Methylene blue; Chemical activation

1. Introduction

Because of unique surface chemistry and textural characteristics activated carbon (AC) has always been a center of attraction for environmental and energy scientists. Phase (solid/liquid and solid/gas) separation and catalysis are among the major environmental applications of AC. In recent years, ligno-cellulosic biomass (LCB) has emerged as a cost effective, eco-friendly, and renewable precursor material for AC, surpassing fossil, non-renewable precursors viz. coal and petroleum pitch. Besides, LCB produces highly pure non-graphitizable char with appropriate hardness and bulk density.

The preparation of AC involves pyrolysis of LCB at moderate temperature under an inert condition to release volatile matters and produce char. Subsequently, the resulting char is activated. Physical and chemical processes are commonly employed for activation [1]. In physical activation, the char is thermally gasified with steam, CO_2, air, or their mixtures to selectively eliminate more reactive carbon atoms of their structure generating well-developed pores [2]. During

* Corresponding author.

chemical activation, chemical is impregnated into the interior of LCB precursor by (solid-solid or solid-liquid) mixing. The impregnated LCB precursor is thermally decomposed. The products evolved during thermal decomposition reacts with impregnated chemical, reducing evolution of volatile matter and inhibiting pores shrinkage, resulting in development of AC with high surface area and well-developed pores [3]. Comparatively low pyrolysis temperature, shorter activation time, high AC yield, and well developed microporosity are the major merits of chemical activation [4]. Alkaline hydroxides viz. NaOH and KOH are commonly used for LCB chemical activation [5]. Among them, NaOH is a better activating agent for carbon precursors with poor structural order, while KOH is better for structurally ordered materials [6]. Thus, structural organization of precursor material is important to be considered while selecting alkaline activation agent.

Date palm tree (*Phoenix dactylifera L.*) is a major cash crop of Arabian Peninsula. The estimated global dried date fruit production is 3.1 million tons/annum, primarily from North African and Middle East countries [7]. Saudi Arabia alone account for about 14% of the total world date production [8]. Substantial amount of agricultural waste in the form of date pits (DPs) has been generated every year as a byproduct of date fruit processing creating waste disposal issue. Thus, converting waste DPs to AC provides a meaningful and sustainable waste utilization solution. Table 1 summarized previously reported DPs activation conditions to AC, surface properties, and adsorbate removed from aqueous phase [9–17]. To our best of knowledge, there is no systematic comparative study on preparation of AC from DPs using both KOH and NaOH as chemical activation agents. Therefore, the aim of this research was to conduct a comparative study to select better activating agent for DPs among KOH and NaOH by optimizing activation conditions viz. impregnation ratio and temperature to obtain high yield date pits activated carbon (DPAC) with better methylene blue (MB) adsorption capacity.

2. Materials and methods

2.1. Chemical and reagents

1,000 mg/L MB stock solution was prepared by dissolving 1,000 mg of MB dye purchased from Sigma-Aldrich, Germany in 1 L of deionized (D.I) water. Alkaline metal hydroxide viz. sodium hydroxide (NaOH) and potassium hydroxide (KOH) used during Date Pit Char (DPC) activation were purchased from Merck, Germany. Hydrochloric acid (HCl) was purchased from Sigma-Aldrich, Germany. The other chemical and reagents used were of analytical reagent (A.R) grade or as specified.

2.2. Preparation of DPAC

Date pits (DPs) used in this study were locally collected. DPs were washed with D.I water, dried overnight in an oven at 80°C to remove moisture. The dried DPs were mechanically ground and sieved to 250 μm particle size. Two-step activation process was used. In first step, the powdered DPs were carbonized in a furnace at 500°C for 2 h at 20°C/min. heating rate to DPC. In second step, NaOH: DPC were mixed at varied wt.: wt. % ratios (1:1, 2:1, and 3:1). A suspension was made in 10 mL of D.I water/gram of NaOH, constantly stirred over magnetic stirrer for 6 h. Samples were dried in an oven at 100°C for 24 h. To activate DPC, samples were kept in a boat shaped crucible and were consecutively placed in a tubular furnace, heated to 650°C–800°C at 20°C/min heating rate for 1.5 h under 100 mL/min nitrogen flow, cooled to room temperature inside a tubular furnace. The obtained DPAC samples were washed several times with 0.1 M HCl until they attain pH ~ 1, the DPAC samples were further washed with hot D.I water until they achieve pH ~ 6.5. The DPAC samples were separated by using 0.45 μm cellulose membrane filters and dried in an oven at 110°C for 24 h. In a similar fashion DPC was mixed with KOH at varied wt.: wt. % ratio and activated. The obtained samples were classified in Table 2.

Table 1
Summary of DPs activation condition, surface analysis, adsorbate removed, and their adsorption capacity

Activation process		Activation conditions			Surface analysis			Adsorbate/adsorption capacity (mg/g)	References
Physical	Chemical	Temp. (°C)	Time (h)	Impregnation ratio	BET surface area (m^2/g)	Total pore volume (cm^3/g)	pH_{PZC}		
–	NaOH	600	1	1:3	1282.5	0.66	7.06	Methylene blue/612.1	[9]
–	H_3PO_4	450	–	1:1.5	54.93	0.015	–	Cd^+/4.29	[10]
–	H_3PO_4	500	2	1:3	873	0.791	–	Malathion/10.46	[11]
–	$FeCl_3$	707	1.27	1.6:1	780.1	–	–	Phenol/97.96	[12]
–	$ZnCl_2$	717	0.5	0.5:1	1045.6	–	–	Phenol/86.11	[12]
N_2	–	700	4	50% N_2 + 50% H_2O	1467	0.725	–	Fe^{3+}, Cu^{2+}	[13]
Steam	–	800	1	–	702	0.321	–	Zn^{2+}/1594, Co^{2+}/1317.52, Pb^{2+}/1261.03, Fe^{3+}/1555.2.	[14]
CO_2, N_2	–	700	2	–	782	0.51	–	4-chlorophenol/390	[15]
N_2	H_3PO_4	500	1	1:1				O-Nitrophenol/142.9 P-Nitrophenol/108.7	[16]
N_2, CO_2	KOH	850	2	1:3	763.4	0.424		2,4-D/238.10	[17]

Table 2
Experimental conditions for DPAC samples preparation, % yield, and amount of MB adsorbed

Sample	Impregnation ratio (wt.: wt. %) (X:DPC)	Activation		% Yield	MB adsorption	
		Temperature (°C)	Time (h)		% Adsorption	Adsorption capacity (mg/g)
Activating agent (X) – NaOH						
DPAC1	3:1	600	1.5	–	6.95	6.95
DPAC2	3:1	650	1.5	–	4.30	4.30
DPAC3	1:1	700	1.5	–	9.8	9.8
DPAC4	2:1	700	1.5	–	16.33	16.33
DPAC5	3:1	700	1.5	–	14.35	14.35
DPAC6	1:1	750	1.5	–	44.89	44.89
DPAC7	2:1	750	1.5	–	91.2	91.2
DPAC8	3:1	750	1.5	58.37	100	100
DPAC9	1:1	800	1.5	–	70.27	70.27
DPAC10	2:1	800	1.5	–	50.81	50.81
DPAC11	3:1	800	1.5	56.77	100	100
DPAC12	3:1	850	1.5	42.48	100	100
DPAC13	–	500	1.5	–	0.49	0.49
X – KOH						
DPAC14	3:1	750	1.5	68.17	99.67	99.67
DPAC15	3:1	800	1.5	57.89	99.77	99.77
DPAC16	3:1	850	1.5	47.62	100	100

2.3. Characterization of DPAC

BET surface area analyzer (Micromeritics, Model ASAP 2020, USA) was used to determine surface area, pore size and pore volume of DPAC11. The surface morphology and elemental composition of DPC and DPAC11 was determined by scanning electron microscope (SEM, Zeiss Supra 35 VP, Germany) coupled with energy dispersive X-ray (EDX, FEI Quanta 450 FEG, Netherland). Fourier-transform infrared (FT-IR) spectrometer (Shimadzu IR Prestige–21, Japan) was used to verify the functional groups present on DPAC11 surface before and after MB adsorption. Point of zero change (pH_{PZC}) of DPAC11 was determined by adopting salt addition method.

2.4. Adsorption studies

Batch mode adsorption studies were conducted in 250 mL Erlenmeyer flasks. 0.10 g of DPAC11 was equilibrated with 100 mL MB solution of initial concentration (C_0) 100 mg/L on isothermal water bath shaker at 120 rpm and 303 K. At equilibrium, the samples were filtered by Whatman filter paper No 41 and residual MB concentration was determined using UV-Visible Spectrophotometer (Shimadzu, Model 1601, Japan) at λ_{max}–665 nm. Effect of MB solution pH on adsorption was studied for range 3–13. Contact time studies were carried out for time range 1–1,440 min at varied MB C_0 viz. 25–200 mg/L and temperatures–303 K. Isotherm and thermodynamic studies were also carried out for C_0 range 25–300 mg/L and temperature range 303–323 K. The MB adsorption capacities at equilibrium and at time t and % adsorption were determined as:

$$q_e(mg/g) = (C_0 - C_e) \times \frac{V}{m} \quad (1)$$

$$q_t(mg/g) = (C_0 - C_t) \times \frac{V}{m} \quad (2)$$

$$\%\ \text{adsorption} = \frac{C_0 - C_e}{C_0} \times 100 \quad (3)$$

where V is the volume of solution (L), m is the mass of DPAC11(g), C_0, C_e and C_t are the initial, equilibrium, and at time t concentrations of MB in aqueous solution, respectively.

3. Results and discussion

3.1. Optimization of DPAC preparation parameters

To achieve maximum adsorption capacity for modeled adsorbate, MB and highest % yield of DPAC, DPC activation conditions were optimized by varying physico-chemical parameters viz. activating agent, activating agent impregnation ratio, and temperature. NaOH and KOH were employed to activate DPC at varied impregnation ratios, and activation temperatures. Table 2 listed samples preparation conditions, % yield, and MB amount adsorbed on DPAC samples. DPAC1 to DPAC13 samples were activated by NaOH, while DPAC14 to DPAC16 samples were activated by KOH. During NaOH activation, the impregnation ratio (NaOH: DPC; wt: wt%) was varied from 1:1 to 1:3, while the activation temperature was varied from 600°C to 850°C. Results revealed a profound effect of impregnation ratio and activation temperature on MB uptake and DPAC % yield. Augmenting NaOH

impregnation ratio from 1:1 to 3:1 and activation temperature from 500°C to 800°C showed an enhancement in MB uptake from 0.49 to 100 mg/g, while the maximum observed DPAC yield was 56.77% for DPAC11. During NaOH activation of DPC, the porosity was induced due to hydroxide reduction and DPC char oxidation [18], proceeds as under:

$$6NaOH + 2C \rightarrow 2Na + 2Na_2CO_3 + 3H_2 \quad (4)$$

$$Na_2CO_3 \rightarrow Na_2O + CO_2 \quad (5)$$

$$2Na + CO_2 \rightarrow Na_2O + CO \quad (6)$$

Also, the increase in activation temperature from 500°C to 800°C entailed pores (micro- and meso-) opening due to the breakage of complex molecule generally present in LCB in turn enlarging the average pore diameter. Besides, further increase in activation temperature to 850°C with impregnation ratio 3:1 doesn't alter maximum MB uptake, but a 37% decrease in DPAC yield (DPAC12) was observed due to an increase in C-NaOH and C-CO_2 gasification reaction rate with activation temperature [19].

During KOH activation of DPC, the impregnation ratio (KOH: DSC; wt.: wt. %) was 3:1, while the activation temperature was varied from 750°C to 850°C for aforementioned samples. The MB uptake capacity varied from 99.67 to 100 mg/g with increase in activation temperature. The metallic potassium was formed during KOH activation process of DPAC which diffuses into the internal matrix of carbon widening existing pores and also creating new ones in accordance to equation [20]:

$$6KOH + 2C \rightarrow 2K + 2K_2CO_3 + 3H_2 \quad (7)$$

A 30.14% loss in DPAC yield during KOH activation with increase in activation temperature from 750°C to 850°C was observed due to increase in C-KOH and C-CO_2 reaction rate [21].

Under similar preparation conditions, the MB uptake capacity was slightly higher on NaOH activated DPAC sample (DPAC11) compared to KOH activated DPAC samples (DPAC15), while a slightly higher %Yield for KOH activated DPAC sample (DPAC15) compared to NaOH activated DPAC sample (DPAC11) was observed, agreed well with previously reported results [22]. But considering economic and ecological aspects NaOH activated DPC sample (DPAC11) was selected for adsorption studies.

3.2. Characterization of DPAC11

The elemental compositions of DPC and DPAC11 were determined by EDX analysis. DPC spectrum (Fig. 1(a)) showed presence of C (61.15 wt. %), O (31.03 wt. %), Si (5.20 wt. %) along with other elemental traces. Fig. 1(b) displayed DPAC11 spectrum. The C and O content on DPAC11 was 92.43 wt. % and 5.98 wt. %, respectively revealing an increase in C and a decrease in O contents during activation process. The traces of sodium (red circled) were present on DPAC11

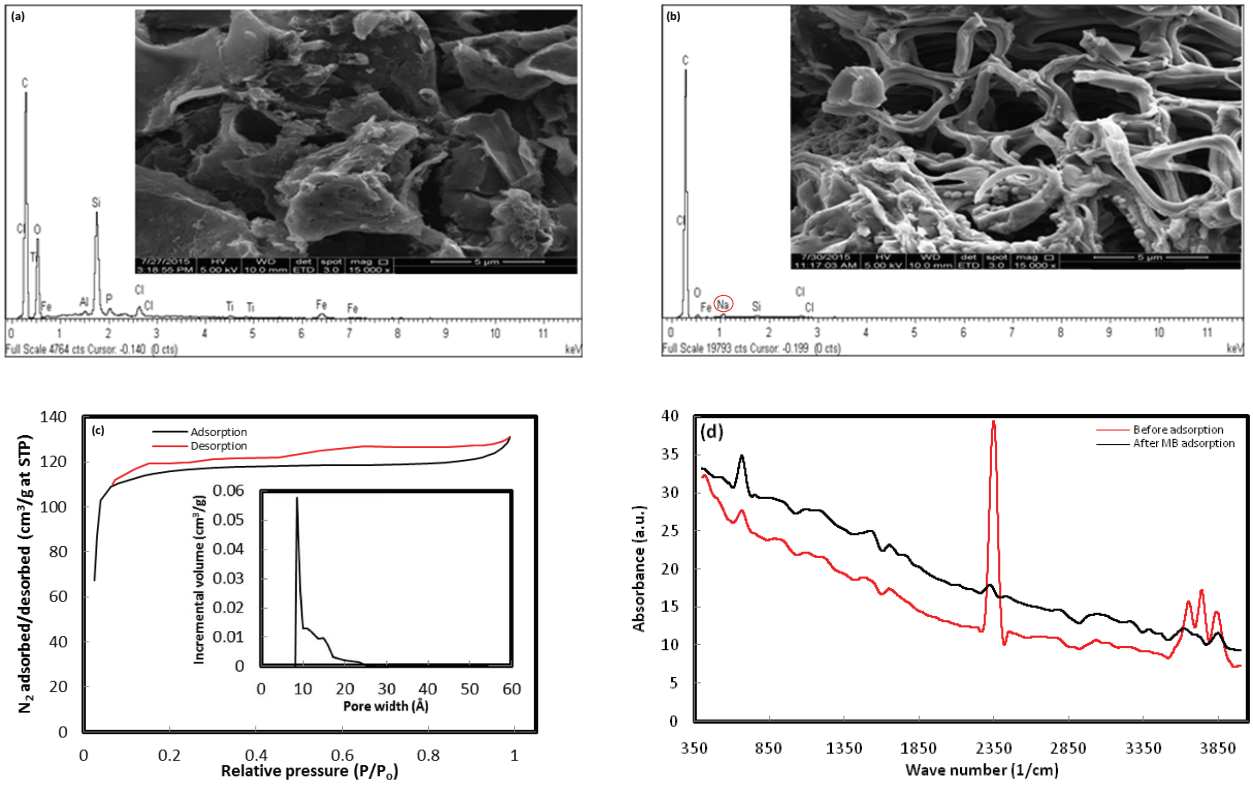

Fig. 1. EDX spectra of DPC (Inset: SEM image) (a), and DPAC11 (Inset: SEM image) (b), Adsorption/desorption isotherm of DPAC11 (Inset: Pore size plot) (c), and FT-IR spectra of DPAC11 (d).

confirming successful activation of char with NaOH, while other trace amount elements were leached out during washing step. The SEM image of DPC (Fig. 1(a), inset) showed irregular surface with some pores developed as volatile matters present on raw DP surface being driven off during carbonization at 500°C. When DPC was infused with AMH, NaOH during activation process a well-organized highly porous DPAC11 surface was developed as left over residues were oxidized and removed (Fig. 1(b), inset). Fig. 1(c) illustrated a type I and II N_2 adsorption/desorption isotherm hybrid exhibiting hysteresis loop at higher relative pressure depicting microporous DPAC11 surface that include a well-developed mesoporous structure [5]. The pore size distribution of DPAC11 as measured by DFT method was in between 8 and 25 Å (Fig. 1(c), inset) with average pore size –21.17 Å featuring mesoporous DPAC11 surface. The BET, Langmuir, and single point (at P/P_o–0.030036) surface areas of DPAC11 were 377.63, 509.85, and 35™, respectively. The total pore volume was 0.0275 cm^3/g. Fig. 1(d) illustrated the FT-IR spectra of DPAC11 before and after MB adsorption. Before MB adsorption, several sharp and strong peaks correspond to the hydroxyl (–OH) group of alcohols and phenols appeared between 3,600 and 3,900 cm^{-1}. A very strong and sharp peak attributed to –OH stretch of strong H-bonded carboxylic (–COOH) group appeared at 2,341 cm^{-1} [23]. Peak at 1,591 cm^{-1} was associated with the stretching vibration in aromatic rings, while a broad peak at 1,456 cm^{-1} was assigned to a typical C–O stretching in carbonate anions [4]. A sharp and strong peak ascribed to the out-of-plane bending vibration of hydroxyl groups appeared at 651 cm^{-1}.The results suggested that carboxyl and hydroxyl groups were the predominant oxygen containing functionalities over DPAC11 surface. These oxygenated functionalities may add polar characteristics to DPAC11 surface [24]. After MB adsorption on DPAC11, peaks at 2,341 cm^{-1} displaced to 2,290 cm^{-1} with a peak size drastically reduced. A peak at 651 cm^{-1} moved to 645 cm^{-1} with reduction in peak size. Also, peaks between 3,600 and 3,900 cm^{-1} disappeared and/or reduced in peak size. The displacement and reduction in peak size confirmed that hydroxyl and carboxyl groups were actively involved for adhering MB ions due to polar and/or electrostatic interactions with DPAC11 surface.

3.3. Adsorption studies

3.3.1. Effect of pH

Solution pH exerts a profound influence on dyes uptake presumably due to its influence on adsorbent surface properties and dyes molecule ionization/dissociation. In this study, MB adsorption on DPAC11 was examined for pH range 3–13. At pH–3, MB adsorption was 111.1 mg/g, attaining maximum MB adsorption (113 mg/g) at pH–9. Above pH 9, a decrease in MB adsorption was observed, reaching minimum MB (105.95 mg/g) uptake at pH–13 (Fig. 2(a)). The observed point of zero charge (pH_{PZC}) for DPAC11 was ~ 8.3 (Fig. 2(b)). The DPAC11 surface was positively charged below pH_{PZC} and negatively charged above pH_{PZC}. Lower MB adsorption at pH–3 may be due to a competition of H^+ ions with cationic MB for the available DPAC11 adsorption sites. As pH gradually increased DPAC11 surface becomes negatively charged favoring enhanced binding of MB ions on DPAC11 surface consequently increasing MB adsorption due to electrostatic attraction. A decrease in MB adsorption on DPAC11 at higher pH (above pH–9) might be subjected to hydrolysis resulting in the creation of positively charged DPAC11 surface sites [25]. Here, it is noteworthy that the overall observed decrease in adsorption capacity for studied pH range was only 6% revealing no significant effect of solution pH on MB removal by DPAC11. Similar MB adsorption trend was observed on dehydrated wheat bran carbon [26], dehydrated peanut hull [27].

3.3.2. Effect of contact time, and initial adsorbate concentration

To optimize equilibration time for MB removal contact time studies were carried out at varied MB initial concentrations (C_0) viz. 25–200 mg/L at 303 K. Fig. 3 showed smooth and continuous plots with comparatively shorter equilibration time (240 to 270 min) at lower C_0 viz. 25 to 100 mg/L. The adsorption on external surface of DPAC11 might be a

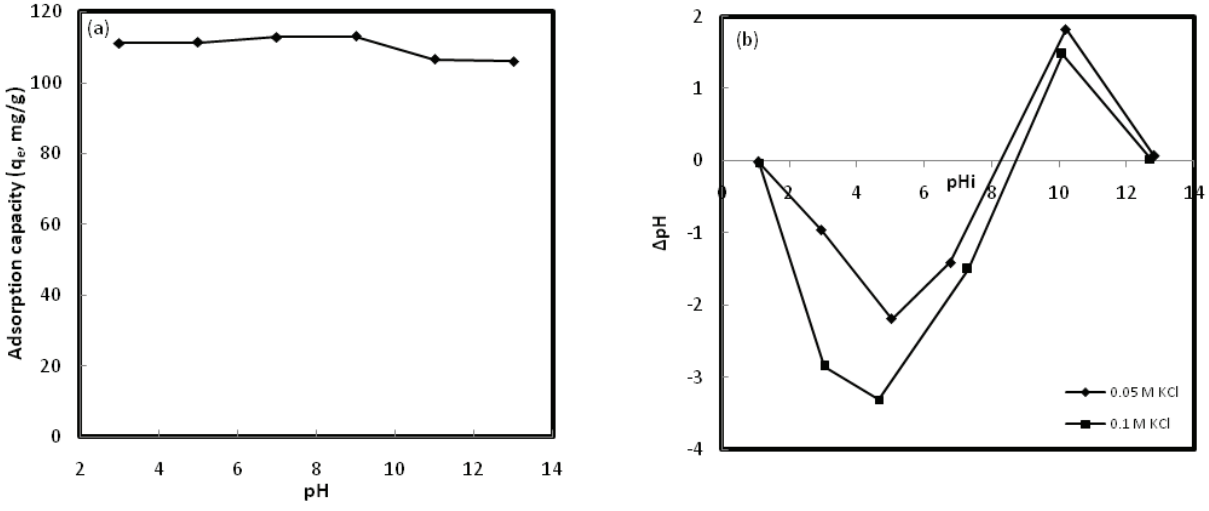

Fig. 2. Effect of pH on MB adsorption onto DPAC11 (a), Point of zero charge plot of DPAC11 (b).

possible reason behind it [28]. The MB uptake capacities at C_0 –25, 50, and 100 mg/L were 20.52, 47.91, and 82.85 mg/g, respectively. At higher C_0 viz. 150 and 200 mg/L, steep slope plots for initial 60 min due to binding of MB onto DPAC11 external surface (faster step) was observed, followed by pore diffusion (slower step) depicted by a decrease in slope, finally attaining equilibrium in 360 and 600 min (Fig. 3). The MB uptake capacities at C_0–150 and 200 mg/L were 100.25 and 124.9 mg/g, respectively. Similar MB adsorption trend on raw DP was observed elsewhere [29].

3.4. Adsorption modeling

3.4.1. Adsorption isotherm models

The two parameters Langmuir and Freundlich isotherm models were applied to adsorption data at varied temperatures. Langmuir isotherm model assumes formation of monomolecular layer during adsorption process without any interaction between adsorbed molecules. The non-linearized and linearized expressions of Langmuir isotherm model are given as [30]:

$$q_e = \frac{q_m b C_e}{1 + b C_e} \tag{8}$$

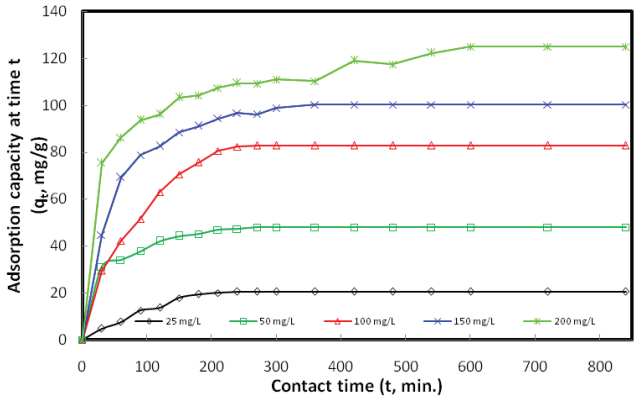

Fig. 3. Effect of contact time on MB adsorption onto DPAC11 at 303 K.

$$\frac{C_e}{q_e} = \frac{1}{K_L q_m} + \frac{1}{q_m} \times C_e \tag{9}$$

where b (L/mg) and q_m (mg/g) are the Langmuir constants for heat of adsorption and maximum solid phase loading on adsorbent surface, respectively.

Freundlich isotherm model assumes occurrence of adsorption process on heterogeneous surface sites. In non-linearized and linearized forms Freundlich isotherm model is expressed as [31]:

$$q_e = K_F C_e^{1/n} \tag{10}$$

$$\log q_e = \log K_F + \frac{1}{n} \log C_e \tag{11}$$

where n and K_F ((mg/g)(L/mg)$^{1/n}$) are Freundlich constants.

The data was analyzed and compared by employing both linear and non-linear isotherm models. Comparatively higher regression coefficient (R^2) values for both linear and non-linear models at varied temperatures were observed for Langmuir isotherm model (Table 3) depicting better fitting of Langmuir model to experimental data, agreed well with previous reports on MB and orange II adsorption onto AC derived from DPs [32] and bimetallic chitosan particle [33], respectively. Additionally, these results were well supported by non-linear adsorption isotherm plots at varied temperatures (Fig. 4) indicating homogeneous monolayer coverage of MB over DPAC11 surface. An increase in q_m-values with increase is temperature from 303 to 323 K was observed. The rise in the kinetic energy of adsorbate ions in aqueous phase with temperature causes an increase in the collision frequency between DPAC11 and MB which is responsible for enhanced MB adsorption on DPAC11 [34]. Also, with increase in temperature the bonds present on DPAC11 surface were ruptured increasing the number of adsorption sites actively involved in adsorption process.

3.4.2. Adsorption kinetic models

The kinetics data at varied MB concentrations was modeled by pseudo-first-order kinetic, pseudo-second-order kinetic and Weber-Morris intra-particle models. Pseudo-first-order kinetic [35] and pseudo-second-order kinetic

Table 3
Adsorption isotherm parameters for MB adsorption on DPAC11

Isotherm model Parameters	Temperature					
	30°C		40°C		50°C	
	Linear	Non-linear	Linear	Non-linear	Linear	Non-linear
Langmuir						
q_m (mg/g)	100	104.02	120.48	119.28	149.25	146.29
K_L (L/mg)	0.074	0.058	0.093	0.097	0.101	0.101
R^2	0.9956	0.9999	0.9983	0.9999	0.9972	0.9998
Freundlich						
K_F (mg/g) (L/mg)$^{1/n}$	16.98	22.32	21.92	29.07	26.98	35.06
n	2.87	3.49	2.88	3.59	2.80	3.45
R^2	0.9509	0.9997	0.9404	0.9998	0.9553	0.9998

[36] and Weber-Morris intraparticle diffusion models in [37] linearized form are expressed as:

$$\log(q_e - q_t) = \log q_e - \frac{k_1}{2.303} \times t \quad (12)$$

$$\frac{t}{q_t} = \frac{1}{K_2 q_e^2} + \frac{1}{q_e} \times t \quad (13)$$

$$q_t = K_{WM} t^{1/2} + I \quad (14)$$

where K_1 (1/min), K_2 (g/mg-min), and K_{WM} (mg/g-min$^{1/2}$) are pseudo-first-order, pseudo-second-order, and intra-particle diffusion rate constants, respectively, I is the intercept related to boundary layer effect.

Table 4 presented adsorption kinetics data. Higher regression coefficient (R^2) and nearer $q_{e,\text{exp.}}$ and $q_{e,\text{cal}}$ values supported better fitting of pseudo-second-order kinetics model at varied concentrations and temperatures. Weber-Morris (WM) intra-particle diffusion plots showed multi-linearity (bi- and tri-linear plots for concentration ranges 25–100 and 150–200 mg/L, respectively (Figure not shown)) and were not passing through the origin showing that other mechanisms along with intra-particle diffusion were governing MB adsorption on DPAC11. The increase in K_{WM} values with the increase in initial MB concentration from 25 to 200 mg/L was observed because higher number of MB molecules in aqueous phase largely attains the active sites on DPAC11 surface. The boundary layer thickness I increased with increase in initial MB concentration attributed to a greater effect of the boundary layer at higher MB concentration [38].

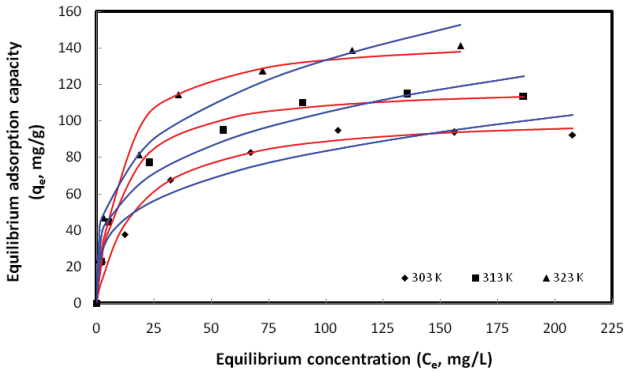

Fig. 4. Non-linear adsorption isotherms for MB adsorption onto DPAC11 (Blue lines – Freudlich isotherm; Red lines – Langmuir isotherm).

3.4.3. Adsorption thermodynamics

The MB adsorption on DPAC11 at varied concentration increases with increase in temperature from 303 to 323 K (Fig. 5). The thermodynamic parameters such as Gibb's free energy change ($\Delta G°$), standard enthalpy change ($\Delta H°$), and standard entropy change ($\Delta S°$) for MB adsorption on

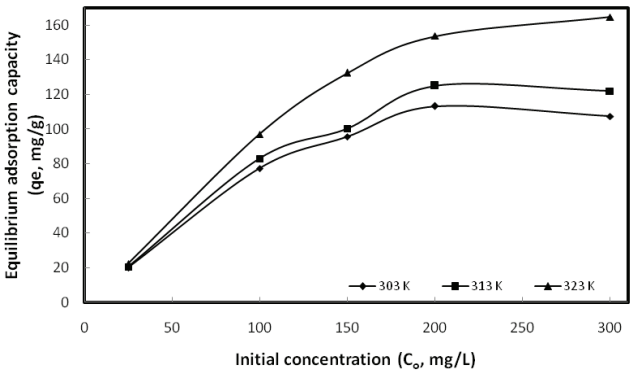

Fig. 5. Effect of temperature on MB adsorption onto DPAC11.

Table 4
Kinetic parameters for MB adsorption at varied concentration on DPAC11

Kinetic model	Initial MB concentration (C_0, mg/L)				
Parameters	25	50	100	150	200
$q_{e,\text{exp}}$ (mg/g)	19.92	41	77.2	95.59	113.15
Pseudo-first-order					
$q_{e,\text{cal}}$ (mg/g)	23.26	51.34	78.2	80.78	58.95
K_1 (1/min.)	0.0405	0.0219	0.0104	0.0106	0.0019
R^2	0.9873	0.9786	0.9774	0.9947	0.8905
Pseudo-second-order					
$q_{e,\text{cal}}$ (mg/g)	20.16	42.91	80	99	113.63
K_2 (g/mg-min.)	0.0091	0.0010	0.0005	0.0004	0.0002
R^2	0.9970	0.9981	0.9992	0.9996	0.9985
Weber-Morris intraparticle diffusion					
K_{WM} (mg/g-min$^{1/2}$)	0.1505	0.6744	2.000	2.0562	2.3613
I	16.754	26.389	31.187	48.893	52.375
R^2	0.3376	0.5400	0.7830	0.7002	0.8396

Table 5
Thermodynamics parameters for the adsorption of MB on DPAC11

Initial MB concentration (C_0, mg/L)	$\Delta S°$ J/mol	$\Delta H°$ kJ/mol	$\Delta G°$, J/mol-K		
			30°C	40°C	50°C
25	21.19	6.182	–5129.33	–5931.69	–7796.85
100	5.82	1.678	–2190.69	–3334.80	–4449.46
150	4.57	1.342	–886.90	–1548.31	–3527.18
200	2.14	0.612	–182.19	–856.94	–2017.87
250	1.48	0.423	845.103	103.52	97.36
300	1.06	0.304	1661.91	1105.05	97.57

DPAC11 were evaluated. Van't Hoff's equation was used to evaluate $\Delta H°$ and $\Delta S°$ expressed as:

$$\ln K_c = \frac{\Delta S°}{R} - \frac{\Delta H°}{R} \times \frac{1}{T} \quad (15)$$

$$K_c = \frac{C_{Ae}}{C_e} \quad (16)$$

where R (8.314 J/mol-K) is a universal gas constant, T (K) is the absolute temperature, K_c is standard thermodynamics equilibrium constant, C_{Ae} (mg/L) and C_e (mg/L) are the equilibrium concentrations of MB on DPAC11 and in aqueous phase, respectively.

The standard free energy change ($\Delta G°$) was evaluated by expression:

$$\Delta G° = -RT \ln K_c \quad (17)$$

Table 5 summarizes thermodynamics parameters for MB adsorption at varied concentration on DPAC11. The adsorption process was endothermic, depicted by positive $\Delta H°$ values at varied MB concentrations. The $\Delta H°$ values decreases with increase in initial MB concentrations revealing that adsorptive forces weakened with concentration. The positive $\Delta S°$ values suggested randomness at solid/solution interface leading to structural changes between MB and DPAC11 during adsorptive interaction. For MB concentration range 25–200 mg/L, the $\Delta G°$ values were negative, decreases with increase in temperature, revealing spontaneous adsorption process and spontaneity increases with temperature. For 250 and 300 mg/L MB concentrations, the $\Delta G°$ values were positive reflecting the presence of energy barrier in the adsorption process, decreases with increase in temperature.

4. Conclusions

In conclusion, NaOH was selected as an activating agent over KOH, with highest % yield and maximum MB adsorption at impregnation ratio – 3:1 and activation temperature – 800°C. A well-organized highly porous DPAC11 with BET surface area–377.63 mg/g was developed by chemical activation. Carboxyl and hydroxyl are the oxygen containing groups dominated over DPAC11 surface adding polar characteristic to surface. For assigned pH range 3–13 a 6% decrease in adsorption proved DPAC11 effectiveness for MB removal under both acidic and basic conditions. The observed equilibration time for C_0 range 25–200 mg/L was in between 240 and 600 min. The adsorption process was endothermic, with homogeneous monolayer MB coverage over DPAC11 surface having maximum MB adsorption capacity–141.25 mg/g at 323 K. Hence, it could be concluded that the developed DPAC11 from DPs is a green and sustainable adsorbent for effective removal of MB from aqueous phase.

Acknowledgement

The authors would like to extend their sincere appreciation to the Deanship of Scientific Research at King Saud University for funding this work through the Research group No. RG-1437-031.

References

[1] F. Rodríguez-Reinoso, M. Molina-Sabio, Activated carbons from lignocellulosic materials by chemical and/or physical activation: an overview, Carbon, 30 (1992) 1111–1118.
[2] H. Marsh, J.L. Figueriredo, J.A. Moulijn, Carbon and Coal Gasification, Martinus Nijhoff, Dordrecht, Netherlands, 1986, p. 27.
[3] M. Smisek, S. Cerny, Active carbon. Manufacture, properties and applications, Elsevier, Amsterdam, 1970.
[4] M.A. Lillo-Ródenas, D. Cazorla-Amorós, A. Linares-Solano, Understanding chemical reactions between carbons and NaOH and KOH: an insight into the chemical activation mechanism, Carbon, 41 (2003) 267–275.
[5] M.A. Khan, Z.A. Al Othman, M. Kumar, M.S. Ola, M.R. Siddique, Biosorption potential assessment of modified pistachio shell waste for methylene blue: thermodynamics and kinetics study, Desal. Wat. Treat., 56 (2015) 146–160.
[6] E. Raymundo-Piñeroa, P. Azaïs, T. Cacciaguerra, D. Cazorla-Amorós, A. Linares-Solano, F. Béguin, KOH and NaOH activation mechanisms of multiwalled carbon nanotubes with different structural organization, Carbon, 43 (2005) 786–795.
[7] A. Alshuaibi, The economics of investment in date production in Saudi Arabia, Int. J. Appl. Econ., 5 (2011) 177–184.
[8] C.-R. Zhang, S.A. Aldosari, P.S.P.V. Vidyasagar, P. Shukla, M.G. Nair, Health-benefits of date fruits produced in Saudi Arabia based on in vitro antioxidant, antiinflammatory and human tumor cell proliferation inhibitory assays, J. Saudi Soc. Agric. Sci., (2015). doi: 10.1016/j.jssas.2015.09.004
[9] M.A. Islam, I.A.W. Tan, A. Benhouria, M. Asif, B.H. Hameed, Mesoporous and adsorptive properties of palm date seed activated carbon prepared via sequential hydrothermal carbonization and sodium hydroxide activation, Chem. Eng. J., 270 (2015) 187–195.
[10] N. Chaouch, M.R. Ouahrani, S. Chaouch, N. Gherraf, Adsorption of cadmium (II) from aqueous solutions by activated carbon produced from Algerian dates stones of *Phoenix dactylifera* by H_3PO_4 activation, Desal. Wat. Treat., 51 (2013) 2087–2092.

[11] A.A. El-Kady, H.H. Abdel Ghafar, M.B.M. Ibrahim, M.A. Abdel-Wahhab, Utilization of activated carbon prepared from agricultural waste for the removal of organophosphorous pesticide from aqueous media, Desal. Wat. Treat., 51 (2013) 7276–7285.
[12] S.K. Theydan, M.J. Ahmed, Optimization of preparation conditions for activated carbons from date stones using response surface methodology, Powder Technol., 224 (2012) 101–108.
[13] C. Bouchelta, M.S. Medjram, M. Zoubida, F.A. Chekkata, N. Ramdanea, J.-P. Bellat, Effects of pyrolysis conditions on the porous structure development of date pits activated carbon, J. Anal. Appl. Pyrol., 94 (2012) 215–222.
[14] N.S. Awwad, A.A. El-Zahhar, A.M. Fouda, H.A. Ibrahium, Removal of heavy metal ions from ground and surface water samples using carbons derived from date pits, J. Environ. Chem. Eng., 1 (2013) 416–423.
[15] M.L. Sekirifa, S. Pallier, M. Hadj-Mahammed, D. Richard, L. Baameur, A.H. Al-Dujaili, Measurement of the performance of an agricultural residue-based activated carbon aiming at the removal of 4-chlophenol from aqueous solutions, Energy Proc., 36 (2013) 94–103.
[16] H. Altaher, A.M. Dietrich, Characterizing o- and p-nitrophenols adsorption onto innovative activated carbon prepared from date pits, Water Sci. Technol., 69 (2014) 31–37.
[17] B.H. Hameed, J.M. Salman, A.L. Ahmad, Adsorption isotherm and kinetic modeling of 2,4-D pesticide on activated carbon derived from date stones, J. Hazard. Mat., 163 (2009) 121–126.
[18] O. Pezoti, A.L., Cazetta, Bedin, C. Karen, L.S. Souza, A.C. Martins, T.L. Silva, O.O. Santos Júnior, J.V. Visentainer, V.C. Almeida, NaOH-activated carbon of high surface area produced from guava seeds as a high-efficiency adsorbent for amoxicillin removal: kinetic, isotherm and thermodynamic studies, Chem. Eng. J., 288 (2016) 778–788.
[19] G.G. Stavropoulos, A.A. Zabaniotou, Production and characterization of activated carbons from olive-seed waste residue, Microporous Mesoporous Mater., 82 (2005) 79–85.
[20] K.Y. Foo, B.H. Hameed, Microwave-assisted preparation and adsorption performance of activated carbon from biodiesel industry solid reside: influence of operational parameters, Bioresour. Technol., 103 (2012) 398–404.
[21] Z.Z. Chowdhury, S.M. Zain, R.A. Khan, A. Arami-Niya, K. Khalid, Process variables optimization for preparation and characterization of novel adsorbent from lignocellulosic waste, BioResources, 7 (2012) 3732–3754.
[22] V. Fierro, V. Torné-Fernández, A. Celzard, Methodical study of the chemical activation of Kraft lignin with KOH and NaOH, Microporous Mesoporous Mater., 101 (2007) 419–431.
[23] C. Lu, C. Liu, G.P. Rao, Comparisons of sorbent cost for the removal of Ni^{2+} from aqueous solution by carbon nanotubes and granular activated carbon, J. Hazard. Mater., 151 (2008) 239–246.
[24] W.T. Tsai, C.Y. Chang, M.C. Lin, S.F. Chien, H.F. Sun, M.F. Hsieh, Adsorption of acid dye onto activated carbons prepared from agricultural waste bagasse by $ZnCl_2$ activation, Chemosphere, 45 (2011) 51–58.
[25] O. Hamdaoui, Batch study of liquid-phase adsorption of methylene blue using cedar sawdust and crushed brick, J. Hazard. Mater., B135 (2006) 264–273.
[26] A. Özer, G. Dursun, Removal of methylene blue from aqueous solution by dehydrated wheat bran carbon, J. Hazard. Mater., 146 (2007) 262–269.
[27] D. Özer, G. Dursun, A. Özer, Methylene blue adsorption from aqueous solution by dehydrated peanut hull, J. Hazard. Mater., 144 (2007) 171–179.
[28] L.S. Oliveira, A.S. Franca, T.M. Alves, S.D.F. Rocha, Evaluation of untreated coffee husks as potential biosorbents for treatment of dye contaminated waters, J. Hazard. Mater., 155 (2008) 507–512.
[29] F. Banat, S. Al-Asheh, L. Al-Makhadmeh, Evaluation of the use of raw and activated date pits as potential adsorbents for dye containing waters, Process Biochem., 39 (2003) 193–202.
[30] I. Langmuir, The adsorption of gases on plane surface of glass, mica and platinum, J. Am. Chem. Soc., 40 (1916) 1361–1403.
[31] H.M.F. Freundlich, Over the adsorption in solution, J. Phys. Chem., 57 (1906) 385–470.
[32] G. Asgari, B. Ramavandi, S. Sahebi, Removal of a cationic dye from wastewater during purification by *Phoenix dactylifera*, Desal. Wat. Treat., 52 (2014) 7354–7365.
[33] G. Asgari, B. Ramavandi, S. Farjadfard, Abatement of Azo Dye from wastewater using bimetal-chitosan, Sci. World J., 2013 (2013) 1–10. doi: 10.1155/2013/476271
[34] M.A. Khan, M. Ngabura, T.S.Y. Choong, H. Masood, L.A. Chuah, Biosorption and desorption of Nickel on oil cake: batch and column studies, Bioresour. Technol., 103 (2012) 35–42.
[35] S. Lagergren, About the theory of so-called adsorption of soluble substances. K. Sven. Vetenskapsakad. Handl., 24 (1898) 1–39.
[36] Y.S. Ho, G. McKay, The kinetics of sorption of divalent metal ions onto sphagnum moss peat, Water Res., 34 (2000) 735–742.
[37] W.J. Weber, J.C. Morris, Kinetics of adsorption on carbon from solution, J. Sanit. Eng. Div. Proceed. Am. Soc. Civil Eng., 89 (1963) 31–59.
[38] W. Cheah, S. Hosseini, M.A. Khan, T.G. Chuah, T.S.Y. Choong, Acid modified carbon coated monolith for methyl orange adsorption, Chem. Eng. J., 215–216 (2013) 747–754.